Innovative Food Science and Emerging Technologies xxx (xxxx) xxx

Contents lists available at ScienceDirect

Innovative Food Science and Emerging Technologies

journal homepage: www.elsevier.com/locate/ifset

The influence of agitation on aroma release

Martijn Weterings [a,b], Igor Bodnár [c], Remko M. Boom [b], Michael Beyrer [a,*]

[a] Institute of Life Technologies, University of Applied Sciences and Arts Western Switzerland, Rue de l'Industrie 19, 1950 Sion, Switzerland
[b] Food Process Engineering Group, Wageningen University and Research Centre, PO Box 18, 6700 AA Wageningen, the Netherlands
[c] Firmenich S.A., Rue de la Bergère 7, 1217 Meyrin-Satigny, Switzerland

ARTICLE INFO

Keywords:
Food process modelling
Mechanistic modelling
Aroma release dynamics
Mass transfer
Aroma release kinetics

ABSTRACT

We have developed a new methodology for measuring aroma release by coupling together two high performance instruments, a proton-transfer-reaction mass spectrometer and closed-cell pressure-controlled rheometer. In this article we report the aroma release from aqueous solutions as a function of different agitation levels, in connection with the theoretical model of mass transfer across interfaces. Two aspects are described in more detail: (1) the use of model parameters to fit the aroma release curves, and (2) the underlying theoretical model in terms of the separate mass transfer coefficients for the liquid phase and the gas phase, including the dependency of these mass transfer coefficients on agitation.

As expected from classical theories, the mass transfer coefficient for the liquid phase was found to correlate with agitation of the liquid phase following a power law relation. The overall aroma release was found to be related to a combination of factors: the thermodynamic equilibrium partition coefficient, as well as the mass transfer coefficient for the liquid phase (at low agitation levels) and the mass transfer coefficient for the gas phase (at high agitation levels).

Industrial relevance: The use of modelling based on the dynamics and mechanistic aspects of aroma release enables a better understanding of the aroma release in real life, and therefore a shorter development cycle for new products. Currently, many experimental studies on aroma release underexpose the need for understanding the dynamics and mechanistic aspects of mass transfer. The new methodology with more accurate measurements and more robust fitting is essential for obtaining experimental data that can be fitted with details of mass transfer models. Furthermore, the experimental system and approach can be used directly in an empiric way for the optimization of the aroma impact and profile of new food products.

1. Introduction

Aroma is an important characteristic and quality factor of food products. Appetizing smell, balanced flavour, and flavour richness are among the major product characteristics that define the palatability of food (Klosse, Riga, Cramwinckel, & Saris, 2004). Knowledge to control and influence this quality aspect is useful to perfect our smell and gustatory senses and to increase the enjoyment of food and eating (Brillat-Savarin, 1862). In the recent years process and product design has gained more impact on food production, with increase in both the means (higher computational capacity) and demand (more consumer-led market with shorter product cycles) (Bruin & Jongen, 2003). Also, the production philosophy is changing, involving more flexibility in the use of raw products, and increasing the complexity of the food chain (van der Goot et al., 2016). These developments require faster and better evaluations of the food product performance and would benefit from predictive insight rather than time consuming tests based on trial and error. This makes knowledge about the dynamics of aroma release and the relevant interactions with the food composition more important.

During food production, aroma release equates to aroma loss which is mostly related to a negative impact on food quality with loss of flavour richness and a distorted flavour balance. The utility of studies on aroma release during production is improvement of technologies and methods that help to control and increase aroma retention, which increases flavour performance during consumption.

Early research on aroma loss and retention started in the late 60s by several chemical engineering research groups who focused on various drying techniques, most importantly spray drying and freeze drying (Coumans, Kerkhof, & Bruin, 1994). Since the 90s aroma release has been studied more widely due to developments in online mass

* Corresponding author.
E-mail address: michael.beyrer@hevs.ch (M. Beyrer).

https://doi.org/10.1016/j.ifset.2021.102610
Received 22 December 2017; Received in revised form 5 January 2021; Accepted 5 January 2021
Available online 12 January 2021

spectrometry measurement techniques (Lindinger, Hansel, & Jordan, 1998; Linforth & Taylor, 1996). Mathematical models that can be used for selecting flavourings have been developed based on multidisciplinary knowledge (de Roos, 2007; Sonnenberg et al., 2002).

The work by de Roos (2006) specifically focusses on the optimization of aroma performance in relation to retention during food processing and proposes three solutions. Besides two technological solutions, encapsulation, and in-situ flavour generation, a solution is found in improving formulations based on modelling and calculations. Yet, despite the theoretical knowledge of fundamental principles of mass transfer, the systems are often complex with many different interactions, and the theoretical knowledge is not that often used (Ammari & Schroen, 2018). Consequently, there is not sufficient knowledge about the details of the influence of process parameters on aroma release during food processing. The necessary parameters are mostly determined on an ad-hoc basis, and the research may sometimes be conflicting, resulting in little consensus on the relevance of the effects of mass transfer (Weterings, Bodnár, Boom, & Beyrer, 2020).

In this report we address the experimental assessment of the aroma mass transfer dynamics during food processing. In Section 2.1 we summarize previous research, which rarely place the experiments into a theoretical framework. In Section 2.2 we summarize this framework as is used for describing our sets of experiments (described in Section 3) that measure the dynamic release of aromas as a function of stirring speed. The fitting procedure with the theoretic model is described in Section 4. We make use of a range of aroma release attributes, the initial release rate, the peak height, the total release, and the depletion rate after the peak has been reached. This generates a robust outcome of mass transfer coefficients, which are then discussed in Section 5. The knowledge on the mass transport dynamics allows us to understand the system and make quantitative predictions for practical purposes.

2. Background

2.1. Experimental frameworks

In recent decades much research has focussed on the challenge of measuring aroma release under dynamic conditions. Many different methods currently exist with various characteristics. In the following list we summarize these methods in increasing order of sophistication and complexity of measurement (We mostly refer to in-vitro methods of analysis. For more detail about in-vivo methods, the interested reader may find more information in the reviews and book chapters: Taylor and Linforth (2010); Romano (2016); Regueiro, Negreira, and Simal-Gandara (2017)):

- *A single measurement at a single time*. This does not provide much information about the kinetics. On the other hand, many analytical techniques can be applied. A recent example is the analysis of release from wine, modelled in-vitro in a bioreactor, using solid phase micro extraction determining head space concentration levels of 44 components simultaneously (Munõz-Gonzáles et al., 2014).
- *Measurements at different times with a separate sample for each selected time*. Comparable to the previous technique but repeated with multiple samples, each of which at a different incubation time (Juteau-Vigier et al., 2007; Mao, Boiteux, Roos, & Miao, 2014; Mao, Roos, & Miao, 2014; Seuvre, Philippe, Rochard, & Voilley, 2007; Tamaru, Ono, Igura, & Shimoda, 2019). This method provides some information about temporal behaviour, but the time resolution is low, and the technique requires many samples to be prepared.
- *Measurements at different times with a single sample extracted multiple times*. This reduces the need of preparing many samples. The increased number of measurement points per test also improves the statistical power. Specialized systems are built for the purpose of obtaining the multiple extractions by directing a stripping gas flow to several trapping stages (Kfoury, Landy, & Fourmentin, 2019; Rabe, Krings, Banavara, & Berger, 2002; Roberts & Acree, 1995).
- *Continuous measurement by dynamic head space dilution*. After equilibration of a sample and the head space above it, the head space is purged by a gas flow that is directed to a mass spectrometer that allows continuous measurement of the dynamic conditions in the head space. The method allows the analysis of release kinetics in liquids (Marin, Baek, & Taylor, 1999, 2000; Taylor et al., 2010; Tsachaki et al., 2008; Tsachaki, Linforth, & Taylor, 2009). The method is also used for more general comparison of (dynamic) head space aroma concentrations above different products, such as testing variations in aroma delivery systems (Fisk, Linforth, Taylor, & Gray, 2011) or variations in different emulsions (Pu, Linforth, Dragosavac, & Wolf, 2019).
- *Continuous measurement by dynamic stripping*. Like the previous technique but the sample is not necessarily at equilibrium prior to connecting the purging gas flow. A sample is placed into a cell after which the head space is stripped with a gas flow that is directed to a mass spectrometer. Early designs of systems to perform this kind of experiment have been made by Lee (1986) and Elmore and Langley (1996). With modern mass spectrometry techniques the method allows accurate comparisons of aroma release in slightly different situations, for instance analysis of variations between different bulking agents at similar viscosity levels (Siefarth et al., 2011) or emulsions with various fat content and droplet size (Frank, Appelqvist, Piyasiri, & Delahunty, 2012).
- *Combined continuous measurement and extractions at different time*. Combined systems have been created to make use of both high time resolution with continuous in-line measurements and wide applicability of analytical techniques with single extractions (Lindinger et al., 2005).
- *On-line systems*. The above techniques have been applied to aroma release dynamics in more complex conditions. The most prominent applications are in-vivo measurement of aroma release during consumption (Regueiro et al., 2017; Romano, 2016; Taylor & Linforth, 2010) and measurements in model systems mimicking the consumption process the mouth (Hinderink, Avison, Boom, & Bodnár, 2019; Ruth & Roozen, 2000), the throat (Weel et al., 2004), or a process as tooth brushing (Pozo-Bayon et al., 2010). On-line measurements have also been applied to study coffee during roasting (Yeretzian, Jordan, Badoud, & Lindinger, 2002) and brewing (Sánchez-López, Zimmermann, & Yeretzian, 2014).
- *Diffusion through layers*. A very specific device for measurement of aroma release was developed by Déléris, Atlan, Souchon, Marin, and Tréléa (2008): A layer of a sample product is placed on top of a membrane and a diffusion process occurs from the bottom of the layer to the head space all above the layer. Accurate estimates of the solubility, the permeability and the diffusivity can be made by varying the thickness of the product layer.

Aroma release is by definition dynamic, and the dynamic nature cannot be neglected. The models applied along with the different measurement methods have dependencies on the mass transfer that may be analysed from a mechanistic point of view. However, only a few studies have analysed the underlying mass transfer models.

2.2. Theoretical frameworks

2.2.1. Two phase model

The head space dilution method has been used to estimate mass transfer coefficients, and analyse underlying mass transfer models for aroma mass transfer from a liquid product to head space (Marin et al., 1999, 2000; Taylor et al., 2010; Tsachaki et al., 2008, 2009). In these analyses the transfer across the interface has been described by the two phase model of Lewis and Whitman (1924) for gases of intermediate solubility, in which an overall mass transfer coefficient, k_o, is the sum of

two separate liquid and gas film transport coefficients, k_l and k_g:

$$\frac{1}{k_0} = \frac{1}{k_l} + \frac{H}{k_g} \quad (1)$$

where H is the molar partition coefficient between the liquid and gas phase, which we will refer to as Henry's coefficient in the rest of this paper since we are dealing with water as liquid phase and air as gas phase.

The influence of process conditions on the individual mass transfer coefficients is typically studied in the field of chemical engineering, for example analysing volumetric mass transfer coefficients, k_la and k_ga, in a bubble column (Besagni, Inzoli, & Ziegenhein, 2018; Schuhfried, Romano, Märk, & Biasioli, 2016). Relationships were found for the mass transfer coefficients and the bubble velocity, $u : k_ga \propto u^{0.75}$ *and* $k_la \propto u^{0.75}$.

2.2.2. Mass transfer correlations

We know by the Buckingham-Π-theorem (Buckingham, 1914) that the relation that describes the mass transfer dependency on other quantities can be reduced to a simple expression in terms of three dimensionless quantities. This simple expression is $Sh = f(Re, Sc)$ with Sh the Sherwood number, Re the Reynolds number, and Sc the Schmidt number. In many works the used expression is a power law function:

$$Sh \propto Re^n Sc^m \quad (2)$$

in which the parameters n and m are determined from correlations in large experimental data sets or based on theoretical considerations.

Only in one set of experimental works on aroma release the results were compared with a mass transfer correlation. These experiments were made with the computerized aroma extraction system of Rabe et al. (2002). Estimates were made of mass transfer coefficients at the liquid/gas interface of water (Banavara, Rabe, Krings, & Berger, 2002), sugar solutions (Rabe, Krings, & Berger, 2003a) and salt solutions (Rabe, Krings, & Berger, 2003b). The correlation used was a correlation function describing mass transfer at the wall interface for turbulent flow in pipes described in various chemical engineering textbooks (Coulson, Richardson, Backhurst, & Harker, 1996; Cussler, 2009; Welty, 2008):

$$Sh = 0.023 Re^{0.83} Sc^{1/3} \quad (3)$$

However, this correlation was adjusted with an additional permeability factor for which there was no theoretical or experimental basis. Also, the correlation itself was not tested by varying the independent parameters in a wide range. In a later study (Rabe, 2004) the stirring rate was varied but no test of the stirring rate dependency was made and the variations in release rate, as function of stirring rate, were explained by disturbance of the surface and increase of the surface area.

The correlation for turbulent flow in pipes in Eq. (3) is just one of many specific versions of Eq. (2). Depending on the geometry and flow regime different power-law coefficients m and n are found. Correlations that are related to the release of aroma from a liquid food product to the head space are summarized in Table 1. In this table we see a range of values for the coefficients m and n in which m is often around 1/3 or 0.5 and n ranges from 1/3 for laminar flow to 0.8 for turbulent flow, and up to around 3 for an aeration process in which the gas becomes vigorously mixed with the liquid. The power law coefficient associated to the Schmidt number, n, has also been associated to theoretical models of the mass transfer at the interface, with $n = 0$ for a model that assumes the interface to be composed of a stable laminar layer, and $n = 0.5$ for a model that assumes the interface to be composed of a continuously replenished dynamic layer (Weterings et al., 2020).

2.2.3. Mechanistic model fits

Mechanistic models have been applied as well to in-vivo systems. An early implementation by Normand, Avison, and Parker (2004) made use of a model based on a mass balance between three phases: saliva, mucosa, and air. The output of this model are estimates from fits for the overall mass transfer rates between the phases.

$$k_{saliva,air} = 0.3{*}10^{-2}[m/s] \text{ and } k_{saliva,mucosa} = 1.7{*}10^{-5}[m/s]$$

More recently such modelling has been done with eight different phases including saliva, mucosa, and air in the oral, pharynx and nasal cavities (Déléris, Saint-Eve, Saglio, Souchon, & Trelea, 2016). Five parameters were used as free parameters in a fitting procedure with two mass transfer coefficients among the results:

$$k_{saliva} = 6.0{*}10^{-5}[m/s] \text{ and } k_{mucosa} = 4.9{*}10^{-5}[m/s]$$

The advantage of these complex models is that they give insights in the effects of many parameters that are not easily tested experimentally. A disadvantage of these complex models is that they provide less stable fits with estimates of lower reliability, while the models are so flexible that they will easily adapt to the data, and thus their value for mechanistic interpretation is limited.

Table 1
Diffusion coefficients of aroma molecules in water and air.

Aroma molecule	Diffusion coefficient in water D_w $*10^{-10}$ [$m^2\ s^{-1}$] (Hayduk and Laudie, 1974)	Diffusion coefficient in air D_g $*10^{-6}$ [$m^2\ s^{-1}$] (Fuller, Schettler, & Giddings, 1966)	Henry's constant H_{bond} [c_l/c_g] (US EPA, 2012)
Ethyl acetate	9.5	8.7	105.0
Ethyl propionate	8.54	7.9	79.2
Ethyl butyrate	7.78	7.2	59.7
Ethyl pentanoate	7.19	6.7	44.9
Ethyl hexanoate	6.70	6.3	33.8

2.3. Robust measurement of mass transfer parameters in aroma release problems

In this report, the aroma release is described by a practical approach of the full theory, simplified to an intuitive as well as mathematical description of aroma release from aqueous solutions. This approach improves the confidence in the used models and in the estimates of the parameters involved. The performance of mechanistic models used to be limited by small amount of experimental data from well controlled studies and lack of knowledge about the system behaviour in experimental settings. This can now be surpassed by increasing computational power and data greedy calculations that start from first principles and fundamental parameters rather than relying on experimental values and on non-reliable estimates.

3. Materials and methods

3.1. Chemicals

The following chemicals were used in this study: Five ethyl esters (ethyl acetate, ethyl propionate, ethyl butyrate, ethyl pentanoate and ethyl hexanoate) were provided by Firmenich SA. Dimethyl sulfoxide (DMSO), was obtained from Sigma Aldrich (> 99.9% purity).

From these chemicals, pre-diluted mixtures of the five ethyl esters, 40 μL each, were made in 10 mL DMSO. DMSO is used because it is a versatile solvent and it dissolves well in water and other food matrices. Another advantage of DMSO is that it has a high boiling point and does not evaporate much, such that it does not interfere with the detection in the PTR-MS.

Descriptive parameters for the five esters are shown in Table 2. The differences between molecules are largest for ethyl acetate: ethyl

Table 2
Concentration of the aroma in the final sample mixture.

Compound	Molarity [μM]	Concentration [mg/L]
Ethyl acetate	7.35	0.648
Ethyl propionate	6.70	0.684
Ethyl butyrate	5.87	0.682
Ethyl pentanoate	5.32	0.682
Ethyl hexanoate	4.91	0.708

hexanoate and results in about a factor 1.5 for the diffusion coefficients and a factor 3 to 4 for the partition coefficient.

3.2. Equipment

3.2.1. Food processing in a rheometer pressure cell

A pressure cell of a MCR302 rheometer (Anton Paar GmbH, Austria) was chosen as a reactor for mimicking food processing, which creates a platform that allows a wide range of parameters to be controlled and measured. In the study described here we used the system to control the stirring rate and temperature. For temperature control the rheometer was equipped with a Peltier system (C-PTD200) and a water bath.

The pressure cell has a cylindrical shape with a 27 mm inner diameter. A cross vane of 24.5 mm width is used for applying physical stress and creating agitation. The cross-vane blades leave a gap of 9 mm at the bottom and 1.25 mm at the edges. The 17 mL sample reaches a height of 32.2 mm, which is 4.2 mm above the top of the vane blades. Such a vane, with flat blades, generates a flow pattern of liquid moving radially outward away from the blades generating two vortexes, one below the blade and one above the blade (Zlokarnik, 1999). The stirring speeds were kept sufficiently low such that no deformation of the surface occurred.

3.2.2. Concentration measurement by PTR-MS

The gas phase aroma concentration was measured by a PTR-MS instrument (IONICON Analytik GmbH, Austria), which was connected to the rheometer pressure cell. The PTR-MS settings were chosen to reduce fractionation of the molecules, preventing an overlap in the spectra from fractions of different aroma molecules. This was done by selecting a low electric field intensity in the reaction tube (around 106 Td) and a low water gas flow towards the ion source (6 sccm). At these setting we found that the fractionation of the ethyl esters is below 1%, which corresponds with findings of Aprea, Biasioli, Märk, and Gasperi (2007).

The reaction tube settings were 450 V, 2.0 mbar pressure and 50 °C. The nose-cone voltage of the inlet to the quadrupole was set at 5.7 V which is a standard value from the manufacturer. The O_2^+ signal is below 1% of the H_3O^+ signal. The amount of water cluster ions, $H_3O^+ \cdot nH_2O$, was between 30 and 70% of the primary H_3O^+ signal, which is related to the low intensity setting.

The PTR-MS was connected via an inlet tube made of a 1.3 m length polyether ether ketone capillary with 1 mm inner diameter, and a polyether ether ketone pre-column filter with a 2 μm frit. The inlet tube was kept at 105 °C to prevent absorption of aroma to the inside surface. The capillary inside the PTR-MS was kept at 80 °C which is the value recommended by the manufacturer. A low inlet flux of 35 mL/min was selected to allow the system to measure the head space continuously while causing limited dilution of the head space and system.

3.2.3. Gas flow system

The basic principle of the in-line measurement is a stripping of the air from the head space in the pressure cell, which is pumped through a loop. The stripped air is passed towards the inlet of the PTR-MS for determination of the aroma concentration. This stripping air system can be described by three flows: a stripping flow, a split flow, and a circulating flow. The settings that are used are shown in Fig. 1 and are:

- 4.3 mL/min for the stripping flow as measured and controlled by a mass flow controller (FMA-2403, Omega, Stamford CT).
- 35 mL/min for the flow towards the PTR-MS, which is determined by the resistance in a double capillary inlet system inside the PTR-MS and set manually with a needle valve. The flow is measured by a secondary mass flow meter (GFM, Aalborg, Denmark).
- 288 mL/min for the circulating flow as determined by a valveless piston metering pump (QG400, Fluid Metering Inc., NY) operating at the maximum of its nominal value.

The stripping flow is introduced to allow continuous sampling of the head space concentration. The stripping flow rate is kept low such that there is no fast depletion of the aroma in the sample and the head space. This makes the signal stronger, more stable, and increases the variation in release of different molecules.

The split flow is introduced because operating the PTR-MS requires a larger inlet flow than the small stripping flow can supply. By mixing with an additional flow of air this requirement can be fulfilled without the necessity of a larger stripping air flow.

The circulation flow serves two purposes. First, it increases the flow rate in the system, most importantly in the section between the rheometer and the PTR-MS. This provides a sharper signal with higher time resolution. The flow rate is low only in the small section of about 1 cm that connects the circulation flow circuit with the split flow towards the PTR-MS. Second, the circulating flow allows to change the gas flow conditions in the rheometer cell while keeping the same stripping

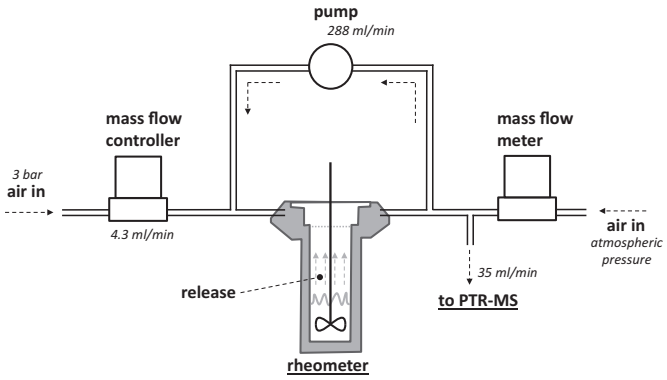

Fig. 1. Schematic overview of the flow system connecting a rheometer pressure cell to a PTR-MS. Aroma release occurs from an aromatized sample into the head space of the rheometer pressure cell. A system of tubes regulates a stripping flow, circulating flow and split flow. This combination of flows ensures that the stripping flow can be kept at a flow 4.3 mL/min while keeping a high 288 mL/min internal flow in the tubes and a large 35 mL/min flow towards the PTR-MS.

flow.

All connections in the flow system were made with polytetrafluoroethylene (PTFE) tubes of 4 mm inner diameter and Swagelok stainless steel connectors. A heating system, set to 25 °C, was placed around the tubes of the flow system. The heating system consists of several independent control loops made with Pt-100 temperature sensors and heating cable wrapped around the tubes. The total volume of the system, pressure cell plus tubes, is 100 mL. The pressure cell volume is 43 mL.

3.3. Sample preparation

An aromatized aqueous solution was used as a food model. This aromatized solution consisted of a mixture of five ethyl esters dissolved in demineralized water. The mixture was made pre-diluting the aroma mixture in DMSO and adding a fraction to the demineralized water. An equilibration period for more than an hour was used before applying samples of the solution in experiments. The concentrations of the aromas in the final mixture were kept below 1% of the maximum solubility and are shown in Table 3.

3.4. Release experiment

An experiment was performed by placing a 17 mL aliquot of the aromatized solution into the rheometer pressure cell and closing the cell. The pressure cell was kept at a temperature of 25 °C. The stirring and the flow system for the aroma concentration measurement were started immediately after loading the sample. From this point on the change of the concentration in the head space was measured by the PTR-MS.

This release experiment measures in a single run the concentrations of the five aroma molecules in the headspace for a period of 80 min with a sample rate of once every four seconds. The runs where repeated 8 times while varying the stirring rate for each repetition (5, 10, 15, 20, 30, 40, 60, and 80 rotations per minute).

The cell was closed manually. During closure of the cell, the gas flow inside the pressure cell is not stable and a short peak and dip are registered for the aroma concentration. A fast initial rise occurs after adding the aroma and before closing the cell. A subsequent decrease occurs after closing the cell. This individual manipulation is not exactly the same from experiment to experiment and it is also not our purpose to analyse these short variations. For the analysis and representation of the results we selected the concentration level after which the release curves in all the experiments are smooth and indicate a stable process.

3.5. Calibration by static head space measurements

In a first calibration we relate the PTR-MS signal to calculated aroma concentrations in an equilibrated head space of a sample placed inside a bottle. This calibration was performed each day to ensure that the response of the PTR-MS was stable and that the measurements were in the linear range.

The head space measurements were adapted from a method by Avison, Gruijthuijsen, Pascu, Parker, and Bodnár (2015). We used 200 mL aqueous solutions of the targeted aroma molecules placed in 1 L glass bottles, closed with fluoroplastic caps (out of TpCh260, Duran®), with a small opening for measurements, and equilibrated for over one hour. During the equilibration the opening was closed with aluminium lined tape. The resulting head space concentration was calculated using the Henry coefficients H_{bond} (see Table 2). Dilutions were made to obtain a range of head space concentrations of ~10 ppbv to ~10 ppmv (parts per billion/million by volume). A measurement of the head space was performed by placing the inlet of the PTR-MS through the small opening in the cap of the bottle. In these cases, the gas flow towards the PTR-MS was entering directly the PTR-MS with a flow rate of 35 mL/min. The gas flow system as described in Section 3.2.3 was not used in this calibration setup.

Table 3
Concentration of the aroma in the final sample mixture.

Compound	Molarity [μM]	Concentration [mg/L]
ethyl acetate	7.35	0.648
ethyl propionate	6.70	0.684
ethyl butyrate	5.87	0.682
ethyl pentanoate	5.32	0.682
ethyl hexanoate	4.91	0.708

3.6. Calibration by full evaporation technique

A second calibration was performed based on full depletion of the aroma in a sample, which was done by fully stripping a sample over a long period (six hours). This is slower because of the time required to evaporate and measure the entire sample. The advantage is that the signal can be directly related to the amount of added aroma rather than to a calculation based on Henry's coefficients from literature correlation functions, or experiments, which do not always have high accuracy. This second calibration is performed with the same inlet system (the flow system, including the split flow setup) as with the experiment, such that there are no influences of changes in the sensitivity of the PTR-MS due to adaptations in the inlet line or changes in humidity.

The total evaporation calibration was performed by running the previously described release experiment overnight, during which nearly all the aroma in the sample evaporated. This signal was then integrated over time and this value was equated to the total quantity of aroma available in the liquid sample that was used for the experiment. The integration of the signal was performed from zero to infinity by applying the integration to a curve that is fitted to the signal.

$$\int_{t=0}^{\infty} signal(t)dt \propto \int_{t=0}^{\infty} \frac{c_g(t)}{c_l(0)}dt = \frac{V_l}{\Phi} \tag{4}$$

For the analysis of the data this second calibration was used. The variation of the second calibration relative to the first calibration was −25%, −13%, −5%, +16% and + 50% for ethyl acetate, ethyl propionate, ethyl butyrate, ethyl pentanoate and ethyl hexanoate respectively. The discrepancy may be due to the different inlet in the first measurement, that is the inlet being directly placed in a bottle rather than connected to the rheometer cell.

4. Analysis

4.1. Mathematical description

A homogeneous concentration of aroma is assumed in the liquid and gas phases separately, in which case a compartmental model can be used to describe the kinetics of the system. The underlying equations of the compartmental model are ordinary differential equations, and their solution is a sum of exponents with an exponential term for each compartment (Godfrey, 1983).

For two compartments, liquid phase, and gas phase, we write the two mass balances, that relate the change of material in the compartments to a term for transport across the interface and a term for transport due to stripping:

$$V_l \frac{dc_l}{dt} = -k_0 A\left(c_l - H_{l/g}c_g\right) \tag{5a}$$

$$\underbrace{V_g \frac{dc_g}{dt}}_{\text{material change}} = \underbrace{k_0 A\left(c_l - H_{l/g}c_g\right)}_{\text{interfacial transport}} - \underbrace{\Phi c_g}_{\text{stripping transport}} \tag{5b}$$

with c_g and c_l the aroma concentration and three type of parameters that describe the physical system: (1) geometrical factors V_g, V_l and A for the gas (head space) volume, liquid (sample) volume and the area at the

interface, (2) dynamic factors Φ and k_O for the air flow rate and the overall mass transfer coefficient, and (3) an equilibrium factor H for the liquid/gas partition coefficient.

A bi-exponential model describes the solution to Eq. (5) and can be used to express the aroma concentration in the gas phase as a time series

$$\frac{c_g(t)}{c_l(0)} = a_1 e^{-b_1 t} + a_2 e^{-b_2 t} = a_1\left(e^{-b_1 t} + e^{-b_2 t}\right) \tag{6}$$

where $\frac{c_g(t)}{c_l(0)}$ is the gas phase aroma concentration made dimensionless by scaling with the liquid aroma concentration at the start, and a_1, a_2, b_1 and b_2 are coefficients. The second equality on the right side of Eq. (6) stems from the application of the boundary condition $c_g(0) = 0$, from which it follows that the coefficients a_1 and a_2 are antisymmetric: $a_1 = -a_2$.

The coefficients a_1, a_2, b_1 and b_2 are related to the parameters that describe the physical system through Eq. (5) (Harrison & Hills, 1997; Weterings et al., 2020):

$$a_1 = -a_2 = \sqrt{H'^2 - 4\xi\beta}^{-1} \tag{7a}$$

$$b_1 = \left(H' - \sqrt{H'^2 - 4\xi\beta}\right)\frac{-k_0 A}{2V_g} \tag{7b}$$

$$b_2 = \left(H' + \sqrt{H'^2 - 4\xi\beta}\right)\frac{-k_0 A}{2V_g} \tag{7c}$$

with dimensionless parameters

$$H' = H + \beta + \xi \tag{8a}$$

$$\beta = \frac{V_g}{V_l} \tag{8b}$$

$$\xi = \frac{\Phi}{k_0 A} \tag{8c}$$

4.1.1. Alternative parametrization

The model coefficients a_1, a_2 (related to the height), b_1 (related to the rate of decline) and b_2 (related to the rate of initial release) are useful for the elegant expression of the Eq. (6) and in a regression analysis. Yet they are just one of many parametrisations and in practice researchers and scientist may use more intuitive coefficients as descriptors of the aroma concentration as function of time. Examples are initial release rate, peak time, peak height, area under the curve, maximum intensity, retention/release after a specific time or ratio of aroma concentration at two time points (Weterings et al., 2020).

In our analysis we will make use of the peak time and peak height as more intuitive coefficients related to the release curves. The peak time and peak height relate to the bi-exponential model coefficients as following:

$$peak\ time = t_{peak} = \frac{ln\left(\frac{a_2 b_2}{a_1 b_1}\right)}{b_2 - b_1} \tag{9a}$$

$$peak\ height = c_{peak} = a_1 e^{-b_1 t_{peak}} + a_2 e^{-b_2 t_{peak}} \tag{9b}$$

4.2. Exponential model fitting procedure

The bi-exponential model is fitted to experimental data by applying a non-linear least squares approximation (Bates & Watts, 1988), using the 'stats' package in R with the default Gauss-Newton algorithm. The initial approximation for the algorithm is made with the algebraic integrative method by Tittelbach-Helmrich (1993). An optimization is made using the mean displacement ratio smoothing method described by Dyson and Isenberg (1971) with QF = 0.8 as smoothing parameter.

Before the experimental measurements start the head space already fills up with aroma when placing the sample into the pressure cell, and the measurement of the aroma release curve does not start at a zero head space aroma concentration: $c_g(0) \neq 0$. The analysis and comparison of results is easier after a shift of the timescales of the release curves such that the condition $c_g(0) = 0$ applies. Therefore, the fitting of data to Eq. (6) is first performed without using the boundary condition '$c_g(0) = 0$' and the time at which the concentration is zero is calculated according to

$$c_g(t_0) = 0 \text{ if } t_0 = \frac{ln(-a_2/a_1)}{(b_2 - b_1)} \tag{10}$$

After a time-translation based on the calculated t0 we obtain $c_g(0) = 0$ and new coefficients a_1 and a_2 that satisfy $a_1 = a_2$.

4.3. Inverse problem: estimating the mass transfer coefficient k_O and partition coefficient H

We can use the concentration measurements to estimate unknown or uncertain physical parameters by using them as fit parameters in the model. This is an inverse problem that uses the relations in Eq. (6) and (7) as shown in the diagram below:

$$\underbrace{\left[\frac{c_g(t)}{c_l(0)}\right]}_{\text{measurements}} \overset{eq.(6)}{\Leftrightarrow} \underbrace{[a_1, a_2, b_1, b_2]}_{\text{model coefficients}} \overset{eq.(7)}{\Leftrightarrow} \underbrace{[V_g, V_l, A, \Phi, k_0, H]}_{\text{physical parameters}}$$

In this report we consider two fit-parameters: k_O and H. For the other parameters V_g, V_l, A and Φ we use their physical values. For the partition coefficient H values could be fixed a priori by using secondary experiments or literature values. However, these values are not precise and small variations between assumed values and real values of H may have a relatively large influence on estimates of k_O due to strong non-linear behaviour near the asymptotes of Eq. (7).

The fitting of the parameters k_O and H is performed via two pathways. A lightweight initial estimate (Section 4.3.1) for k_O and H is made via an indirect two stage regression model. This initial estimate is useful for illustrative purposes and it also acts as a starting condition for a final more complex regression model (Section 4.3.2) that estimates the k_O and H more directly.

4.3.1. Initial fitting of k_O and H to model coefficients

The initial estimation of k_O and H is done in two regression steps. First the bi-exponential model in Eq. (6) is fitted to each individual concentration-time curve to obtain raw coefficients (a_1, a_2, b_1, and b_2). Second the model in Eq. (7) is fitted to these coefficients to obtain the parameters k_O and H.

The procedure is also performed visually by comparing the experimental and calculated values of the pairs of the peak time and peak height (t_{peak}, c_{peak}) by using Eq. (9). This comparison is done visually with a scatter plot (see Fig. 3 later in this report) of the experimentally determined pairs with isolines describing theoretical values based on k_O and H. The pairs associated to a single molecule and food composition are expected to be positioned on a single iso-H-curve and a combination of k_O-values for increasing agitation/stirring rates.

This use of a combination of coefficients, both t_{peak} and c_{peak}, is more robust than correlating k_O to only a single coefficient: for instance, using only a peak value or only an initial release rate in order to estimate k_O. Correlating k_O with only a single coefficient is compromised if small experimental variations in the estimation of coefficients (t_{peak}, c_{peak}) correspond to relatively large errors in estimates of k_O. This occurs especially around asymptotes which are present in all of Eqs. (7a), (7b) and (7c).

4.3.2. Final direct fitting of k_o and H

The final estimation of k_o and H is done in a single regression step. The fitting is made by inserting Eq. (7) into (6) and applying a non-linear least squares algorithm directly to the parameters k_o and H. We use this direct fitting procedure to obtain the final estimated values for k_o and H. The initial estimated values of k_o and H serve as a starting condition that

improves the convergence in this final regression.

4.4. Determination of k_g and k_l

After obtaining values of the overall mass transport coefficient k_o as function of both the aroma type and the stirring rate, an estimate can be made of the gas and liquid film mass transport coefficients, k_g and k_l in the right side of Eq. (1). The Eq. (1) is closed by using the Eq. (2) for the k_g and k_l terms and solving for the scaling factor and the power law exponent related to the Reynolds number. In terms of non-dimensional parameters, the used power-law relationships read

$$Sh_l = A_l Re_l^{n_l} Sc_l^{1/3} \tag{11}$$

$$Sh_g = A_g Re_g^{n_g} Sc_g^{1/3} = B_g Sc_g^{1/3} \tag{12}$$

in which the parameters to be estimated are A_l, B_g, which are scale factors, and n_l is the power law exponent. We absorb $A_g Re_g^{n_g}$ into a single constant parameter B_g, because the effect of agitation in the liquid phase on the flow in the gas phase may be neglected.

The Sherwood number, impeller Reynolds number, Schmidt number in the liquid and gas are

$$Sh_l = \frac{k_l}{D_l/L_l} \tag{13a}$$

$$Sh_g = \frac{k_g}{D_g/L_g} \tag{13b}$$

$$Re_l = \frac{d^2\omega}{\nu_l} \tag{13c}$$

$$Re_g = \frac{d^2\omega}{\nu_g} \tag{13d}$$

$$Sc_l = \frac{\nu_l}{D_l} \tag{13e}$$

$$Sc_g = \frac{\nu_g}{D_g} \tag{13f}$$

in which the subscripts l and g refer to the liquid phase and the gas phase, D is the diffusion coefficient, L is the height of the phase, d is the diameter of the rheometer pressure cell, and ν is the kinematic viscosity. The impeller Reynolds number is varied by changing the stirring rate while the diameter d and the kinematic viscosity ν remain unchanged for each aroma. For the computation of the Schmidt numbers we use textbook values of the kinematic viscosities, $\nu_g = 1.57{*}10^{-5}$ [m^2/s] for the gas (air) phase and $\nu_l = 1.00{*}10^{-6}$ [m^2/s] for the liquid (water) phase. This results in Sc_g values between 1.5 and 3 and Sc_l values between 1000 and 1500.

We do not make an estimate of the exponent related to the Schmidt numbers and fix it to the value 1/3, which is a typical value among correlation functions in the literature (see Table 1). The range of variability in Schmidt numbers in this experiment is very small and the regression line that estimates the power law exponent would be very short such that experimental variations in the error terms would have a relatively large effect on the estimate of the power-law exponent.

It would be more straightforward to insert Eqs. (11) and (12), via Eqs. (2) and (13), into (6) and (7) and directly compute the full model, without first calculating k_O in an intermediate step. However, it is not trivial to achieve convergence with this large model. To reliably express the error for the estimated parameters we evaluated confidence intervals by bootstrapping with thousand-fold re-sampling of the residuals, which does yield correct estimates of the confidence intervals.

5. Results and discussion

5.1. Release curves

The aroma concentrations in the head space of a pressure cell were measured during the release of a mixture of five esters. The experiments were repeated with varying stirring speeds from 5 to 80 [rpm]. For each different aroma molecule and different stirrer speed a different time series, curve, is shown. The results are represented in Fig. 2 with the aroma concentration in the head space as a function of time, aroma type and stirring speed. Qualitative observations are:

- Time: The general picture of a release curve is an increase of the head space aroma concentration during roughly the first half hour. As time progresses the rate of increase decreases and in the second half of the experiment the head space aroma concentration remains equal or even decreases.
- Aroma: A higher aroma head space concentration is observed for aroma molecules with a smaller liquid/gas partition coefficient. The ranking is ethyl hexanoate > ethyl pentanoate > ethyl butyrate > ethyl propionate > ethyl acetate. The observation of this effect is made more salient in Fig. 2 by placing the plots next to each other in order of both increasing relative head space concentration and increasing partition coefficient.
- Stirrer speed: An increase of aroma release is observed for higher stirrer rates. This is observed as both a higher level of the peak or plateau and a shorter time scale at which this level is reached.
- Aroma × stirrer speed: A variation is observed in the change in the peak levels as a function of stirring speed. For the molecules with high liquid/gas partition coefficient the relative change in the levels is much narrower as a function of stirring speed. In the case of ethyl acetate, the distinction between curves of different stirring rates is small.

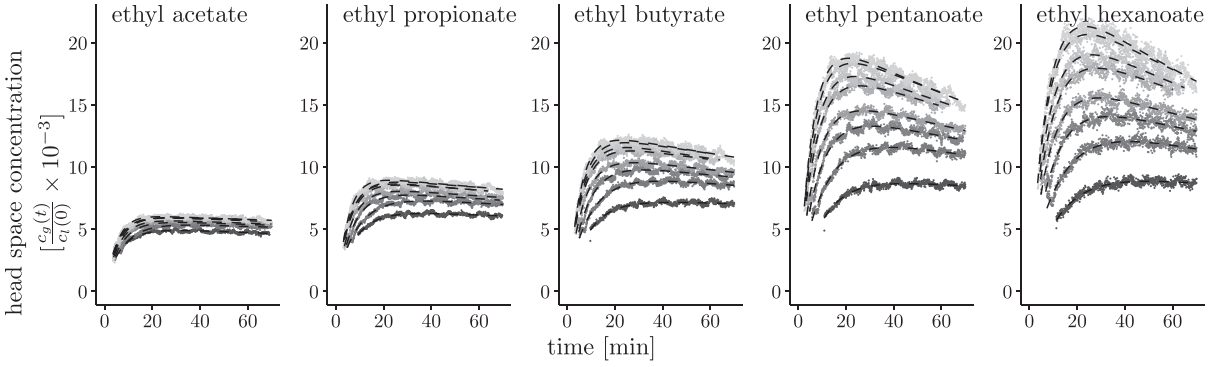

Fig. 2. Release curves, headspace concentration versus time, for five different esters and eight different stirring speeds (from dark to light 5, 10, 15, 20, 30, 40, 60 and 80 [rpm]). The dashed lines are fitted curves based on the multi-exponential model in Eq. (6). To show more clearly the relationship between the partition coefficient and the change in the height of the aroma release curves, the plots for different esters are placed next to each other, ordered by liquid/gas partition coefficient, with the same time and concentration scales.

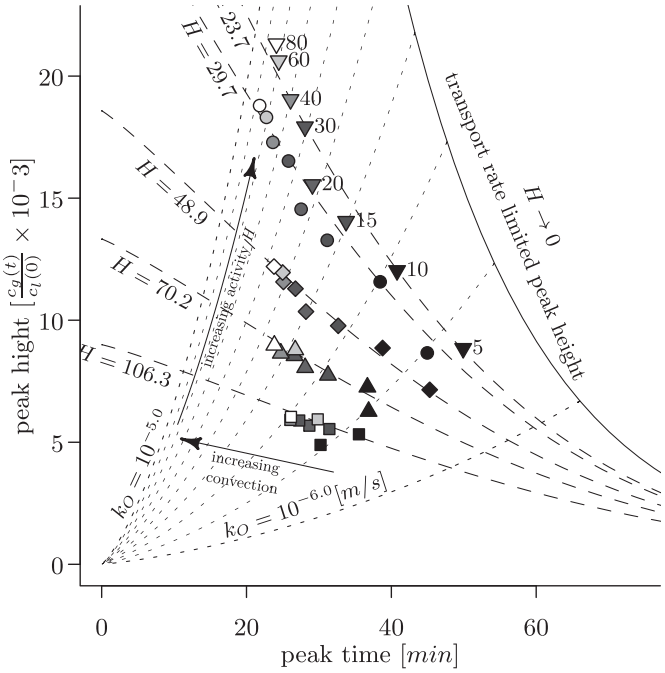

Fig. 3. Scatterplot of pairs (t_{peak}, c_{peak}) for varying stirring speeds (from dark to light 5, 10, 15, 20, 30, 40, 60 and 80 [rpm]) and aroma types (ethyl acetate ∎, ethyl propionate ▲, ethyl butyrate ◆, ethyl pentanoate ●, and ethyl hexanoate ▼).
Iso-H-lines and isok_o-lines are drawn to show the dependence of the pairs (t_{peak}; c_{peak}) on H and k_o, if other variables are kept constant. As expected, the pairs associated to a single molecule are positioned near a single iso-H-curve and on increasing iso- k_o-curves for increasing stirring rates.
The region in the top-right corner is a limit for possible peak height and time. Also, with decreasing partition coefficient $H \to 0$ a boundary is reached, and the properties of peak height and time do not change much further.

5.2. Intuitive interpretation of results

A simple interpretation of the results can be made by contrasting them with the simpler situation of a closed system with a static head space. At this point it is important to note the similarity in the expressions $H+\beta+\xi$ and $H+\beta$ that relate to the heights of the head space aroma concentration in the dynamic case and static case respectively:

$$open\ system-peak\ level \Rightarrow \frac{c_g(t_{peak})}{c_l(0)} \sim (H+\beta+\xi)^{-1} \tag{14}$$

$$closed\ system-static\ steady\ state \Rightarrow \lim_{t\to\infty} \frac{c_g(t)}{c_l(0)} = (H+\beta)^{-1} \tag{15}$$

The expression $H+\beta$ is a fundamental relation in static head space analysis (Kolb & Ettre, 1997) and expresses the effect of the phase ratio on the final head space concentration. The expression $H+\beta+\xi$ is a similar type of summation and includes an extra term ξ that relates to the balance between stripping (gas flow) and replenishment (mass transport from the liquid sample) of the aroma in the head space. The curves in Fig. 2 show that the static expression (15) is not appropriate; the release curves seem to approach a plateau level, but this level is not an equilibrium that depends only on aroma type and phase ratio, and the stirring rate has an important role as well.

5.2.1. Plateau level and decline

The head space aroma concentration does not reach a steady state equilibrium value as in a closed system. In the first part the head space aroma concentration increases towards a peak or plateau level. However, after a peak with no change in the aroma concentration the aroma concentration starts to decline. In most cases this decline is slow, and therefore seemingly resembles a plateau.

The decline can be attributed to the stripping of the head space, which slowly depletes the system and reduces the aroma levels. The rate of this depletion relates to the flux of the stripping flow. Because the flux is kept low the decline is small, but variations are still observable. The relative depletion rate is more noticeable for higher stirring rates and smaller liquid/gas partition coefficients. In these cases, the relative amount of aroma in the head space is larger, and this gives the stripping of the head space a larger effect as a relatively larger fraction of the aroma in the system is stripped.

5.2.2. Stirring rate effect

The peak level is dependent on the stirring rate, and not just on the aroma type as in the Eq. (15) for the static equilibrium value. Also, in all cases the height of the peak or plateau level is below this static equilibrium value.

This difference with the static equilibrium value, which is dependent on the stirring rate, can be explained by the open system not reaching a steady state in the same way as a closed system does. In a closed system a static equilibrium or static steady state is reached when the mass transfer across the interface drops to zero (which happens at equilibrium). On the other hand, in an open system a peak is reached when the mass transfer across the interface balances the mass transfer from the stripping flow. This occurs when the head space aroma concentration is still different from the static equilibrium value in Eq. (15). With higher stirring rates the rate of mass transfer is higher and the mass flux across the interface will be higher for smaller driving forces. With higher stirring rates the head space aroma concentration at the peak level will be closer to the static equilibrium value.

5.3. Peak time and peak height

For each release curve the pairs of peak time and peak height, (t_{peak}, c_{peak}), are plotted in Fig. 3. The values of the pairs were obtained by the

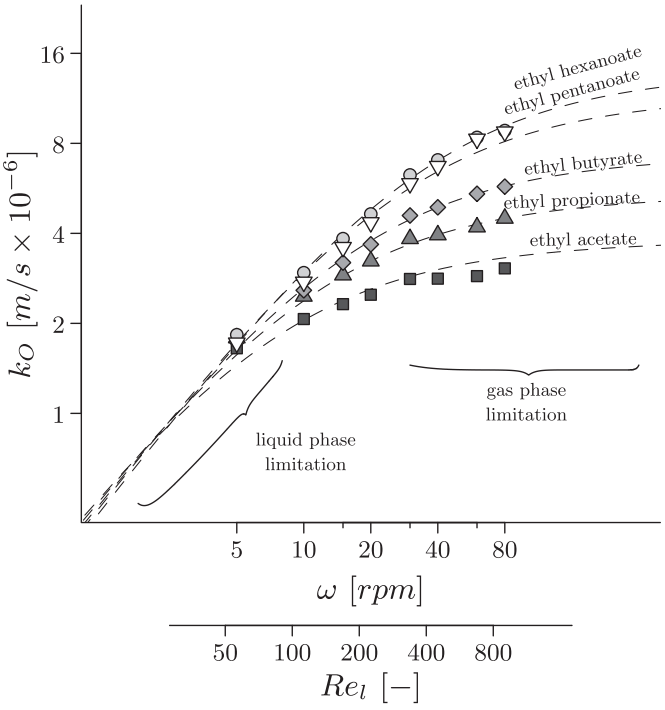

Fig. 4. The overall mass transfer coefficient for various aroma molecules (ethyl acetate ■, ethyl propionate ▲, ethyl butyrate ◆, ethyl pentanoate ●, and ethyl hexanoate ▽) as a function of stirring speed n varied from 5 to 80 rpm.
The dashed lines are fits according to the models in Eqs. (1), (11) and (12) and relate to an impeller Reynolds number dependency of the liquid mass transfer coefficient $k_l \propto Re_l^{n_l}$ with $n_l \sim 1$. At high stirring velocities, the increase in the overall mass transfer reaches a plateau which is due to the influence of the gas phase mass transfer rate. The degree in which the gas phase mass transfer coefficient has influence is related to the partition coefficient (in the term H/k_g) and increases from ethyl hexanoate to ethyl acetate.

multi-exponential fitting procedure described in the Methods Section 4.2. The pairs relate to the curves in Fig. 2 and provide a more condensed representation of these multiple curves.

The measured (t_{peak}, c_{peak})-pairs that belong to a single aroma are positioned in Fig. 3 on a single iso-H-curve. This provides confirmation that the compartment model is able to approximate the system and that the setting the Henry coefficient as a free parameter is not over-fitting the experimental results. The values of the plotted iso-H-curves are chosen based on the values of H that were returned by the direct fitting of parameters k_o and H. In this study we find liquid/gas partition coefficients that are relatively low compared with literature values (described in the Table 2): 24, 30, 49, 70 and 106 for ethyl hexanoate, ethyl pentanoate, ethyl butyrate, ethyl propionate and ethyl acetate respectively. While in the literature (Aprea et al., 2007; Fenclová, Blahut, Vrbka, Dohnal, & Böhme, A., 2014; US EPA, 2012) one finds values up to 50% higher.

Based on the isok_o-lines we see that the values for the overall mass transfer coefficient are between $\sim 2 \cdot 10^{-6}$ and $\sim 9 \cdot 10^{-6}$ [m/s]. These are lower values than found by Déléris et al. (2016) and Normand et al. (2004). They studied both aroma release from samples placed in the mouth, in which case it may be that the resistance in the air layer is lower due to stronger convection. The variation of the mass transfer coefficients, as function of stirring rate, is larger for aroma molecules with decreasing liquid/gas partition coefficient (ethyl acetate < ethyl propionate < ethyl butyrate < ethyl pentanoate ~ ethyl hexanoate), due to the larger dominance of the liquid mass transfer coefficient, and effects of stirring rate, for the molecules with smaller liquid/gas partition coefficient as in Eq. (1).

From Fig. 3 we can also assess how estimates of the mass transfer coefficient may result in relatively large errors if they are based on single fitting parameters and/or external input of the partition coefficient H. For instance, the different (t_{peak}, c_{peak}) values for ethyl acetate have little variance in the peak height whereas the variance in peak times is larger. This means that changes in the mass transfer coefficient relate to relatively small changes of the peak heights. In the inverse case: if there are small changes in the peak heights, due to measurement errors, or if there are wrong estimates of the partition coefficient H, then there will be a large uncertainty in the estimate of the mass transfer coefficient.

5.4. The overall mass transfer coefficient k_o

The overall mass transfer coefficient, k_o, is determined by direct fitting of Eqs. (7) substituted into (6). A plot of the values as function of the stirring rate is shown in Fig. 4. In this plot we also show fitted curves that are based on the two-film model in Eq. (1). These curves relate to the mass transfer coefficients k_l and k_g in the liquid and gas layers which we will discuss in more detail later.

Before we describe the results quantitatively we note that three features in Fig. 4 can already be well described qualitatively: an overall mass transport coefficient that (1) increases with increasing stirring rate (2) to an asymptote and (3) where this asymptote is at a higher overall mass Eq. (11) transport rate for aroma molecules with a smaller liquid/gas partition coefficient.

- Correlation k_o and ω: The increasing curves in the Fig. 4 show that the mass transfer coefficient k_o correlates positively with stirring rate. This is as expected as stirring generally increases the mass transfer by inducing convection in the liquid and maximizes the replenishment of aroma from the bulk to the interface.
- Non-linear behaviour: In Fig. 4 we see that the rate of increase in k_o as a function of stirring rate is smaller at higher stirring rates. This corresponds to a two-layer model in which one part varies with the stirring rate and one other part remains constant or varies much less. In the theory described by Eq. (1) the overall resistance to mass

transfer $\left(\frac{1}{k_o}\right)$ is the sum of a resistance in the liquid side interfacial layer and a resistance in the gas side interfacial layer. At high stirring rates the resistance to mass transfer in the liquid layer decreases while the resistance to mass transfer in the gas layer remains (or decreases much less) and becomes the dominant factor.

- Cross-effect with aroma type: The bend in the curves in Fig. 4 occurs at higher stirring rates, and at higher levels of k_o, for aroma molecules with a lower liquid/gas partition coefficient. This is related to the aroma molecules with a higher liquid/gas partition coefficient being more influenced by the resistance in the gas phase.

This effect may be seen as counter intuitive from the perspective that different aroma molecules have similar diffusion coefficients (for Fick's law). However, it is not the difference in diffusion coefficients, or liquid and gas mass transfer coefficients, that cause the variation in the overall mass transfer coefficient. The reason for more influence of the resistance in the gas layer and a smaller overall mass transfer coefficient is in the driving force. This is because molecules with a high liquid/gas partition coefficient have a large concentration step at the interface resulting in a smaller aroma concentration gradient in the gas phase for the same aroma concentration in the liquid phase. In the limit of a very high mass transport in the liquid phase, the concentration in the gas just near the interface will approach an asymptote equal to the equilibrium value c_l/H. The smaller concentration gradient in the gas phase, due to a smaller concentration just near the interface (the limit c_l/H), can be related to a smaller rate of mass transport for higher H.

The three qualitative observations support a two-film model as described by Eq. (1), and show that three factors, k_l, k_g and H each play a role of importance. With the data from this study a more thorough analysis can be made by quantifying k_l and k_g and determining the dependence of k_l on the stirring rate.

5.5. The separate mass transfer coefficients k_g and k_l

The experimentally derived values of k_o were fitted with the two-film model in Eq. (1) and experimental correlations for k_l and k_g in Eqs. (11) and (12). Curves of the fits are added to the experimental data points in Fig. 4. The fitting parameters n_l, A_l and B_g are shown in Table 4. Table 5 provides an overview, as an easy reference, of the values for mass transfer coefficients and Sherwood numbers at the slowest and fastest stirring rate.

Table 4
Estimates of coefficients for Eqs. (11) and (12). The values between brackets are 95% confidence intervals based on a bootstrapping method with thousand-fold re-sampling of the residuals.

Liquid phase:		Gas phase:	
Eq. (11) $Sh_l = A_l Re_l^{n_l} Sc_l^{1/3}$		Eq. (12) $Sh_g = B_g Sc_g^{1/3}$	
Coefficient and value	95%-confidence interval	Coefficient and value	95%-confidence interval
$n_l = 0.99$	[0.91, 1.10]		
$A_l = 0.15$	[0.09, 0.22]	$B_g = 2.52$	[2.33, 2.69]

The fitted curves match with the data points in Fig. 4. The error in the estimates of the fit-parameters, due to variability of the error terms, is evaluated by bootstrapping with thousand-fold re-sampling of the residuals. If the re-sampling results in similar results (that is, within small variation) then the fit is well conditioned with respect to the error in the data points. This is the case for the parameter n_l which is estimated with a 95%-confidence interval of about ± 0.1 as shown in Table 4.

The coefficients A_l has a large variation with a 95%-confidence levels of about a factor 2 difference of the estimated value. Part of the large variation in the coefficient is because it behaves opposite to the variation in the power law term Re^n which has a large influence for small variations in n (for example $900^{0.9}$ versus $900^{1.1}$ is almost a factor 4 difference).

5.6. Implications of k_g and k_l and variations by stirring rate

The differences between aroma types are small in terms of the liquid and gas Sherwood numbers and mass transfer coefficients (presented in Table 5). This is as expected since the aroma types do not differ much in liquid and gas diffusion coefficients. The largest difference in the estimated liquid mass transfer coefficients is a factor 1.3 difference between ethyl acetate and ethyl hexanoate. At high stirring rates, the differences in the estimated overall mass transfer coefficients are larger, factor 3 difference between ethyl acetate and ethyl hexanoate, and mainly determined by the differences in partition coefficient, which is a factor 4.5 between ethyl acatete and ethyl hexanoate. The partition coefficient occurs in the $\frac{H}{k_g}$term in the Eq. (1) for the two-film model.

The differences between stirring rates are large in the liquid gas phase mass transfer coefficient k_l. The coefficient increases by more than a factor of ten when changing the stirring rate 5 to 80 [rpm], and the value of the power law coefficient n_l was determined at 0.99, which indicates a strong influence of the stirring on the mass transfer rate. The cases for turbulent flow in pipes and over flat plates in Table 1 have $n_l = 0.8$ which is lower. This strong influence of stirring may be due to the high curvature of the flow in the geometry which induces instabilities and strong radial outflow that very effectively replenish the surface layer and increase the impeller flow number (the effectiveness at which the vane pumps liquid around per rotation). In future work the mass transfer might be studied further by incorporating an agitation of the gas phase separately from the agitation in the liquid phase.

The Sherwood numbers for the mass transport in the gas phase are around 3.5 and much smaller than the Sherwood numbers for the mass transport in the liquid phase, which are between 90 and 1800 depending on the stirring rate. The small(er) Sherwood numbers for the transport in the gas phase are as expected and may relate to the smaller Schmidt number which is three orders of magnitude smaller for the gas phase in comparison to the liquid phase. If the low Sherwood numbers in the gas phase are a general phenomenon, or at least more common, then this means that for many systems the mass transport coefficients for the gas phase can be easily and quickly estimated by using an approximation

Table 5
Selected values obtained from fits of Eqs. (11) and (12): k_o, k_l, k_g, Sh_l and Sh_g at stirring rates 5 and 80 [rpm].

Compound	Stirring rate 5 [rpm], $Re = 56$					Stirring rate 80 [rpm], $Re = 901$				
	k_o [m/s]	k_l [m/s]	k_g [m/s]	Sh_l [−]	Sh_g [−]	k_o [m/s]	k_l [m/s]	k_g [m/s]	Sh_l [−]	Sh_g [−]
ethyl acetate	$1.45{\cdot}10^{-6}$	$2.43{\cdot}10^{-6}$	$3.83{\cdot}10^{-4}$	116	4.2	$3.30{\cdot}10^{-6}$	$3.80{\cdot}10^{-5}$	$3.83{\cdot}10^{-4}$	1815	4.2
ethyl propionate	$1.57{\cdot}10^{-6}$	$2.26{\cdot}10^{-6}$	$3.59{\cdot}10^{-4}$	108	4.0	$4.46{\cdot}10^{-6}$	$3.53{\cdot}10^{-5}$	$3.59{\cdot}10^{-4}$	1687	4.0
ethyl butyrate	$1.63{\cdot}10^{-6}$	$2.13{\cdot}10^{-6}$	$3.39{\cdot}10^{-4}$	101	3.7	$5.73{\cdot}10^{-6}$	$3.32{\cdot}10^{-5}$	$3.39{\cdot}10^{-4}$	1587	3.7
ethyl pentanoate	$1.70{\cdot}10^{-6}$	$2.01{\cdot}10^{-6}$	$3.23{\cdot}10^{-4}$	97	3.6	$8.08{\cdot}10^{-6}$	$3.15{\cdot}10^{-5}$	$3.23{\cdot}10^{-4}$	1504	3.6
ethyl hexanoate	$1.68{\cdot}10^{-6}$	$1.93{\cdot}10^{-6}$	$3.09{\cdot}10^{-4}$	92	3.4	$9.09{\cdot}10^{-6}$	$3.00{\cdot}10^{-5}$	$3.09{\cdot}10^{-4}$	1436	3.4

with the ratio D_g/L_g for pure diffusive transport, and ignoring possible variations in agitation.

6. Conclusions

We observed that agitation has a strong and non-linear influence on aroma release. Parameters k_l, k_g and H determine together a change in release behaviour of the different molecules. At low stirring rates the release is dominated by transport in the liquid phase and by the stripping factor and at high stirring rates the release is dominated by transport in the gas phase and by the partitioning coefficient. The changeover point is strongly influenced by the partitioning coefficient.

The variations in separate mass transfer coefficients in the gas and liquid k_g and k_l were not strongly dependent on the aroma type. The overall mass transfer coefficient k_o varied based on variations between aroma types in the partition coefficient H.

The results from this report have several consequences for future aroma release studies and models, that can be summarized as follows:

- There is a large influence of agitation on the outcome of the release experiment. This effect needs to be taken into account in the comparison of different studies.
- The agitation has an influence that varies depending on the type of aroma molecules. This underlines the bi-modal classification system developed in Weterings et al. (2020). In our results we see the switch between different classes. With an increase of the stirring rate a change is seen from liquid layer dominating to gas layer dominating and from static equilibrium dominating to stripping factor dominating.
- The fitting of *dynamic* release curves to a multi-exponential model provides a strong and robust method for creating estimates of parameters that describe the physical system.

Future work may address different processing conditions, different processing types, different food compositions, and different food types. The outcome can subsequently be used to evaluate and refine theories or be used in predictive food modelling. The predictive power can then be evaluated more precisely and at a wider scale.

Acknowledgements

Acknowledgements to Christoph Ellert and Jérémie Bérard for construction of the gas flow system, and to the support of Anton Paar GmbH, and the Commission for Technology and Innovation (CTI) of Switzerland (grant number 14936.1).

References

Ammari, A., & Schroen, K. (2018). Flavor retention and release from beverages: A kinetic and thermodynamic perspective. *Journal of Agricultural and Food Chemistry, 66*, 9869–9881. https://doi.org/10.1021/acs.jafc.8b04459

Aprea, E., Biasioli, F., Märk, T. D., & Gasperi, F. (2007). PTR-MS study of esters in water and water/ethanol solutions: Fragmentation patterns and partition coefficients. *International Journal of Mass Spectrometry, 262*, 114–121.

Avison, S., Gruijthuijsen, K., Pascu, M., Parker, A., & Bodnár, I. (2015). Novel methodology for measuring temperature-dependent Henry's constants of flavor molecules. *Journal of Agricultural and Food Chemistry, 63*, 6313–6318.

Banavara, D. S., Rabe, S., Krings, U., & Berger, R. G. (2002). Modeling dynamic flavor release from water. *Journal of Agricultural and Food Chemistry, 50*, 6448–6452.

Bates, D. M., & Watts, D. G. (1988). *Nonlinear regression analysis and its applications*. Hoboken, NJ, USA: Wiley.

Besagni, G., Inzoli, F., & Ziegenhein, T. (2018). Two-phase bubble columns: A comprehensive review. *ChemEngineering, 2*, 13. https://doi.org/10.3390/chemengineering2020013

Brillat-Savarin, J. A. (1862). *Physiologie du goût*. Paris, France: Charpentier, libraire-éditeur.

Bruin, S., & Jongen, T. R. G. J. (2003). Food process engineering: The last 25 years and challenges ahead. *Compr Rev Food Sci F, 2*, 42–81.

Buckingham, E. (1914). On physically similar systems: Illustrations of the use of dimensional equations. *Physics Review, 4*, 345–376.

Coulson, J. M., Richardson, J. F., Backhurst, J. M., & Harker, J. H. (1996). *Coulson & Richardson's chemical engineering. Fluid flow, heat transfer, and mass transfer volume 1* (6th ed.). Oxford, MA, USA: Butterworth-Heinemann.

Coumans, J. W., Kerkhof, P. J. A. M., & Bruin, S. (1994). Theoretical and practical aspects of aroma retention in spray drying and freeze drying. *Drying Technology, 12*, 99–149.

Cussler, E. L. (2009). *Diffusion mass transfer in fluid systems*. New York, NY, USA: Cambridge University Press.

Déléris, I., Atlan, S., Souchon, I., Marin, M., & Tréléa, I. C. (2008). An experimental device to determine the apparent diffusivities of aroma compounds. *Journal of Food Engineering, 85*, 232–242.

Déléris, I., Saint-Eve, A., Saglio, A., Souchon, I., & Trelea, I. C. (2016). Insights in aroma compound retention by mucosa during consumption through mathematical modelling. *Journal of Food Engineering, 190*, 123–138.

Dyson, R. D., & Isenberg, I. (1971). Analysis of exponential curves by a method of moments, with special attention to sedimentation equilibrium and fluorescence decay. *Biochemistry-us, 10*, 3233–3240.

Elmore, J. S., & Langley, K. R. (1996). Novel vessel for the measurement of dynamic flavor release in real time from liquid foods. *Journal of Agricultural and Food Chemistry, 44*, 3560–3563.

Fenclová, D., Blahut, B., Vrbka, P., Dohnal, V., & Bohme, A.. (2014). Temperature dependence of limiting activity co-efficients, Henry's law constants, and related infinite dilution properties of C4-C6 isomeric n-alkyl ethanoates/ethyl n-alkanoates in water. Measurement, critical compilation, correlation, and recommended data. *Measurement Science and Technology, 4*, 1323–1329.

Fisk, I. D., Linforth, R. S. T., Taylor, A. J., & Gray, D. A. (2011). Aroma encapsulation and aroma delivery by oil body suspensions derived from sunflower seeds (Helianthus Annus). *European Food Research and Technology, 232*, 905–910. https://doi.org/10.1007/s00217-011-1459-z

Frank, D., Appelqvist, I., Piyasiri, U., & Delahunty, C. (2012). In vitro measurement of volatile release in model lipid emulsions using proton transfer reaction mass spectrometry. *Journal of Agricultural and Food Chemistry, 60*, 2264–2273. https://doi.org/10.1021/jf204120h

Fuller, N. E., Schettler, P. D., & Giddings, J. C. (1966). A new method for prediction of binary gas-phase diffusion coefficients. *Industrial and Engineering Chemistry, 58*, 18–27.

Godfrey, K. (1983). *Compartmental models and their application*. London, England: Academic Press.

van der Goot, A. J., Pelgrom, P. J. M., Berghout, J. A. M., Geerts, M. E. J., Jankowiak, L., Hardt, N. A., Keijer, J., Schutyser, M. A. I., Nikiforidis, C. V., & Boom, R. M. (2016). Concepts for further sustainable production of foods. *Journal of Food Engineering, 168*, 42–51.

Harrison, M., & Hills, B. P. (1997). Effects of air flow-rate on flavour release from liquid emulsions in the mouth. *International Journal of Food Science and Technology, 32*, 1–9.

Hayduk, W., & Laudie, H. (1974). Prediction of diffusion coefficients for nonelectrolytes in dilute aqueous solutions. *AICHE Journal, 20*, 611–615.

Hinderink, E. B. A., Avison, S., Boom, R., & Bodnár, I. (2019). Dynamic flavor release from chewing gum: Mechanisms of release. *Food Research International, 116*, 717–723. https://doi.org/10.1016/j.foodres.2018.09.002

Juteau-Vigier, A., Atlan, S., Déléris, I., Guichard, E., Souchon, I., & Trelea, I. C. (2007). Ethyl Hexanoate transfer modeling in carrageenan matrices for determination of diffusion and partition properties. *Journal of Agricultural and Food Chemistry, 55*, 3577–3584.

Kfoury, M., Landy, D., & Fourmentin, S. (2019). Contribution of headspace to the analysis of Cyclodextrin inclusion complexes. *Journal of Inclusion Phenomena and Macrocyclic Chemistry, 93*, 19–32. https://doi.org/10.1007/s10847-018-0818-9

Klosse, P., Riga, J., Cramwinckel, A., & Saris, W. (2004). The formulation and evaluation of culinary success factors (CSFs) that determine the palatability of food. *Food Serv Technol, 4*, 107–115.

Kolb, B., & Ettre, S. L. (1997). *Static headspace-gas chromatography: Theory and practice* (1st ed.). New York, NY, USA: Wiley-VCH, Inc.

Kozinski, A. A., & King, J. C. (1966). The influence of diffusivity on liquid phase mass transfer to the free interface in a stirred vessel. *AICHE Journal, 12*, 109–116.

Lee, W. E. (1986). A suggested instrumental technique for studying dynamic flavor release from food products. *Journal of Food Science, 51*, 249–250.

Lewis, W. K., & Whitman, W. G. (1924). Principles of gas absorption. *Industrial and Engineering Chemistry, 16*, 1215–1220.

Lindinger, C., Hansel, A., & Jordan, A. (1998). On-line monitoring of volatile organic compounds at pptv levels by means of proton-transfer-reaction mass spectrometry (PTR-MS) medical applications, food control and environmental research. *International Journal of Mass Spectrometry, 173*, 191–241.

Lindinger, C., Pollen, P., Ali, S., Yeretzian, C., Blank, I., & Märk, T. (2005). Unambiguous identification of volatile organic compounds by proton-transfer reaction mass spectrometry coupled with GC/MS. *Analytical Chemistry, 77*, 4117–4124.

Linforth, R. S. T., & Taylor, A. J. (1996). Apparatus and methods for the analysis of trace constituents in gases. Patent, US 5869344 A.

Mao, L., Boiteux, L., Roos, Y. H., & Miao, S. (2014). Evaluation of volatile characteristics in whey protein isolate–pectin mixed layer emulsions under different environmental conditions. *Food Hydrocolloids, 41*, 79–85.

Mao, L., Roos, Y. H., & Miao, S. (2014). Flavour release from Monoglyceride structured oil-in-water emulsions through static headspace analysis. *Food Biophysics, 9*, 359–367. https://doi.org/10.1007/s11483-014-9338-3

Marin, M., Baek, I., & Taylor, A. J. (1999). Volatile release from aqueous solutions under dynamic headspace dilution conditions. *Journal of Agricultural and Food Chemistry, 47*, 4750–4755.

Marin, M., Baek, I., & Taylor, A. J. (2000). Flavor release as a unit operation: a mass transfer approach based on a dynamic headspace dilution method. In D. D. Roberts,

& A. J. Taylor (Eds.), *763. Flavor Release* (pp. 153–165). Washington, D.C., USA: American Chemical Society.

Munõz-Gonzáles, C., Feron, G., Guichard, E., Rodríguez-Bencomo, J. J., Martín-Álvarez, P. J., Moreno-Arribas, V. M., & Pozo-Bayón, M. A. (2014). Understanding the role of saliva in aroma release from wine by using static and dynamic headspace conditions. *Journal of Agricultural and Food Chemistry, 62*, 8274–8288.

Munz, C., & Roberts, P. V. (1984). The ratio of gas-phase to liquid-phase mass transfer coefficients in gas-liquid contacting processes. In W. Brutsaert, & G. H. Jirka (Eds.), *Gas transfer at water surfaces* (pp. 33–45). Dordrecht, Netherlands: Springer.

Normand, V., Avison, S., & Parker, A. (2004). Modeling the kinetics of flavour release during drinking. *Chemical Senses, 29*, 235–245.

Pozo-Bayon, M. A., Pimenta, P., Pilch, S., Masters, J. G., Martín-Álvarez, P. J., & Reineccius, G. (2010). API-IT-MS for measuring aroma release from dentifrice products using a device to simulate tooth brushing. *Journal of Agricultural and Food Chemistry, 58*, 5034–5041.

Pu, X., Linforth, R., Dragosavac, M. M., & Wolf, B. (2019). Dynamic aroma release from complex food emulsions. *Journal of Agricultural and Food Chemistry, 67*, 9325–9334. https://doi.org/10.1021/acs.jafc.9b02304

Rabe, S. (2004). In vitro study of the influence of physiological parameters on dynamic in-mouth flavour release from liquids. *Chemical Senses, 29*, 153–162.

Rabe, S., Krings, U., Banavara, D. S., & Berger, G. B. (2002). Computerized apparatus for measuring dynamic flavor release from liquid food matrices. *Journal of Agricultural and Food Chemistry, 50*, 6440–6447.

Rabe, S., Krings, U., & Berger, R. G. (2003a). Dynamic flavor release from sucrose solutions. *Journal of Agricultural and Food Chemistry, 51*, 5058–5066.

Rabe, S., Krings, U., & Berger, R. G. (2003b). Initial dynamic flavour release from sodium chloride solutions. *European Food Research and Technology, 218*, 32–39.

Regueiro, J., Negreira, N., & Simal-Gandara, J. (2017). Challenges in relating concentrations of aromas and tastes with flavor features of foods. *Critical Reviews in Food Science and Nutrition, 57*, 2112–2127. https://doi.org/10.1080/10408398.2015.1048775

Richter, K. E., & Jähne, B. (2010). A laboratory study of the Schmidt number dependency of air-water gas transfer. In S. Komori, W. McGillis, & R. Kurose (Eds.), *Gas transfer at water surfaces 2010* (pp. 266–295). Kyoto, Japan: Kyoto University Press.

Roberts, D. D., & Acree, T. E. (1995). Simulation of Retronasal aroma using a modified headspace technique: Investigating the effects of saliva, temperature, shearing, and oil on flavour release. *Journal of Agricultural and Food Chemistry, 43*, 2179–2186.

Roberts, P. V., & Dändliker, P. G. (1983). Mass transfer of volatile organic contaminants from aqueous solution to the atmosphere during surface aeration. *Environmental Science & Technology, 17*, 484–489.

Romano, A. (2016). Aroma release during in-mouth process. In E. Guichard, C. Salles, M. Morzel, & A.-M. Le Bon (Eds.), *Flavor* (pp. 235–265). Chichester, UK: John Wiley & Sons, Ltd.. https://doi.org/10.1002/9781118929384.ch10

de Roos, K. B. (2006). Understanding and controlling the behaviour of aroma compounds in thermally processed foods. *Trends in Food Science and Technology, 17*, 236–243.

de Roos, K. B. (2007). Selecting the right flavourings for a food product. In A. J. Taylor, & J. Hort (Eds.), *Modifying flavour in food chapter 14* (pp. 243–273). Cambridge, England: Woodhead Publishing Limited.

Ruth, S. M., & Roozen, J. (2000). Influence of mastication and saliva on aroma release in a model mouth system. *Food Chemistry, 71*, 339–345.

Sánchez-López, J. A., Zimmermann, R., & Yeretzian, C. (2014). Insight into the time-resolved extraction of aroma compounds during espresso coffee preparation: Online monitoring by PTR-ToF-MS. *Analytical Chemistry, 86*, 11696–11704.

Schuhfried, E., Romano, A., Märk, T. D., & Biasioli, F. (2016). Proton transfer reaction-mass spectrometry (PTR-MS) as a tool for the determination of mass transfer coefficients. *Chemical Engineering Science, 141*, 205–213.

Seuvre, A.-M., Philippe, E., Rochard, S., & Voilley, A. (2007). Kinetic study of the release of aroma compounds in different model food systems. *Food Research International, 40*, 480–492.

Siefarth, C., Tyapkova, O., Beauchamp, J., Schweiggert, U., Buettner, A., & Bader, S. (2011). Influence of polyolsand bulking agents on flavour release from low-viscosity solutions. *Food Chemistry, 129*, 1462–1468.

Sonnenberg, S., Finke, A., Klamt, A., Lohrenz, J., Burger, T., & Matthiesen, S. (2002). Selection method for aroma substances. Patent, US20020152038A1.

Tamaru, S., Ono, A., Igura, N., & Shimoda, M. (2019). High correlation between octanol-air partition coefficient and aroma release rate from O/W emulsions under non-equilibrium. *Food Research International, 116*, 883–887. https://doi.org/10.1016/j.foodres.2018.09.024

Taylor, A. J., & Linforth, R. S. T. (2010). On-line monitoring of flavour processes. In A. J. Taylor, & R. S. T. Linforth (Eds.), *Food flavour technology* (pp. 266–295). Oxford, United Kingdom: Wiley-Blackwell.

Taylor, A. J., Tsachaki, M., Lopez, R., Morris, C., Ferreira, V., & Wolf, B. (2010). Odorant release from alcoholic beverages. In N. C. Da Costa, & R. J. Cannon (Eds.), *Flavors in noncarbonated beverages chapter 12* (pp. 161–175). Washington, D.C., USA: American Chemical Society.

Tittelbach-Helmrich, K. (1993). An integration method for the analysis of multiexponential transient signals. *Measurement Science and Technology, 4*, 1323–1329.

Tsachaki, A., Gady, M., Kalopesas, M., Linforth, R. S. T., Athè, V., Marin, M., & Taylor, A. J. (2008). Effect of ethanol, temperature, and gas flow rate on volatile release from aqueous solutions under dynamic headspace dilution conditions. *Journal of Agricultural and Food Chemistry, 56*, 5308–5315.

Tsachaki, M., Linforth, R. S. T., & Taylor, A. J. (2009). Aroma release from wines under dynamic conditions. *Journal of Agricultural and Food Chemistry, 57*, 6976–6981.

US EPA. (2012). *Estimation programs interface suite™ for microsoft® windows, v 4.11*.

Weel, K. G. C., Boelrijk, A. E. M., Burger, J. J., Verschueren, M., Gruppen, H., Voragen, A. G. J., & Smit, G. (2004). New device to simulate swallowing and in vivo aroma release in the throat from liquid and semiliquid food systems. *Journal of Agricultural and Food Chemistry, 52*, 6564–6571.

Welty, J. R. (Ed.). (2008). *Fundamentals of momentum, heat, and mass transfer* (5th ed.). Denver, MA, USA: Wiley.

Weterings, M., Bodnár, I., Boom, R. M., & Beyrer, M. (2020). A classification scheme for interfacial mass transfer and the kinetics of aroma release. *Trends in Food Science and Technology, 105*, 433–448.

Yeretzian, C., Jordan, A., Badoud, R., & Lindinger, W. (2002). From the green bean to the cup of coffee: Investigating coffee roasting by on-line monitoring of volatiles. *European Food Research and Technology, 214*, 92–104.

Zlokarnik, M. (1999). *Rührtechnik. Theorie und Praxis* (1st ed.). Berlin, Germany: Springer-Verlag.